Mechanism of Ligand Binding to Ni(II)−Fe(II) Hybrid Hemoglobins†

Naoya Shibayama,‡ Takashi Yonetani,§ Rebecca M. Regan,|| and Quentin H. Gibson*,||

Department of Physics, Jichi Medical School, Minamikawachi-machi, Kawachi-Gun, Tochigi-Ken 329-04, Japan, Department of Biophysics and Biochemistry, University of Pennsylvania, Philadelphia, Pennsylvania 19104, and Department of Biochemistry and Molecular and Cell Biology, Cornell University, Ithaca, New York, 14853

Received June 12, 1995; Revised Manuscript Received August 7, 1995⊗

ABSTRACT: The geminate and bimolecular binding of CO, O_2, and NO to $[\alpha\text{-Ni(II)}]_2-[\beta\text{-Fe(II)}]_2$ and $[\alpha\text{-Fe(II)}]_2-[\beta\text{-Ni(II)}]_2$ hybrid hemoglobins has been studied. Bimolecular reactions: At pH 6.6 and 20° both hybrids bind CO at $0.15 \times 10^6\ M^{-1}\ s^{-1}$. Reactions with oxygen: At pH 6.6 the on rates are 4.8 and $7.5 \times 10^6\ M^{-1}\ s^{-1}$ for α- and β-hybrids, respectively; the off rate is approximately $2 \times 10^3\ s^{-1}$ for both. At pH 8 the α-Fe hybrid shows cooperativity whereas the β-hybrid does not. Nanosecond geminate reactions: Faster bimolecular rates correlate with larger geminate amplitudes; thus α-Fe hybrids have larger amplitudes, and O_2 geminate amplitudes are larger than those with CO. At pH 8, 50% of O_2 recombines with the α-hybrid. With NO, nanosecond geminate recombination is observable only with the β-hybrid. Picosecond reactions: α-Hybrids show picosecond recombination of O_2. With NO, α-hybrids recombine at 30 ns^{-1}, β-hybrids at 0.3 ns^{-1}. The NO picosecond rates correlate with the molecular dynamics which shows ligands leaving the β-Fe atom early and regularly, but remaining near the α-Fe atom. The results may be explained by assuming an interaction between the α-subunits giving rise to a high-affinity fast-reacting form, whereas the β-subunits only become fast-reacting when an R−T conformation change analogous to that of hemoglobin A takes place. A third allosteric state is postulated to explain the results.

Metalloglobins in which nickel porphyrin has been substituted for heme have been studied in some detail. When all four hemes are replaced, only ligand binding to the proximal histidine can be followed. It has also been shown that the Ni protein is tetrameric and that the reactivity of β-93 SH with 4,4-dithiopyridine corresponds to a low-affinity, deoxy, or T-state conformation. (Alston et al., 1984; Shelnutt et al., 1986; Manoharan et al., 1989).

Nickel does not react with O_2, CO, or NO, and as Ni porphyrin binds firmly to the heme site, if it is substituted for specific hemes the ligand binding reactions of the remaining hemes may be studied in isolation. Detailed studies of spectra and oxygen binding of both α- and β-Ni substituted hybrids have appeared (Shibayama et al., 1986).

The crystal structure of the α-Ni substituted hybrid with ligand at the β-hemes has been determined (Luisi et al., 1990), and the structure of the β-Ni hybrid has been compared with that of hemoglobin A (HbA) (Luisi & Shibayama, 1989).

Kinetic studies of CO binding to both α- and β-substituted hybrids have reported large effects of an allosteric transition on bimolecular and nanosecond geminate reactions with similar results in both cases (Murray et al., 1988, 1989).

The object of the present paper is to describe the ligand binding reactions in more detail, extending the time scale of observations to the picosecond range, and examining the behavior of O_2 and NO as ligands. The results are compared with molecular dynamics simulations, and their relation to the two-state model (Monod et al., 1965) is discussed. It is concluded that a third allosteric state is necessary to account for the results.

METHODS

The Ni−Fe hybrid hemoglobins were prepared as described by Shibayama et al. (1986). They were stored at N_2 temperature, and portions were dissolved in the required buffers immediately before the experiments were performed. The buffers used were 0.1 M KP_i at pH 6.6 and pH 7.0 and 0.1 M borate at pH 9.1. Intermediate pH values used 0.1 M Tris-HCl with 0.1 M KCl. Gases were taken from tanks with O_2/N_2 mixtures containing 2.0% and 5.1% O_2, and from a tank with 9.5% CO, as well as 100% O_2 and 100% CO. NO gas was introduced into 100-mL tonometers using a syringe for measurement.

Measurements of bimolecular reaction rates were made by photolyzing solutions in 1-mm cuvettes at a concentration of about 50 μM in Fe using a 9-ns pulse from a Q-switched YAG laser (Continuum Inc., Santa Clara, CA). The beam was reduced to 2 mm in diameter with a telescope. The observation beam from a 75-W Xe arc was collinear with the laser beam. The cuvette was temperature controlled with a Peltier effect chip (Melcor), thermistor, amplifier, and programmable power supply. The output of the photomultiplier was amplified and transferred to a 1-μs conversion time 12-bit A/D board (MetraByte Corp., Taunton, MA, Model DAS-50), collecting 1024 points for each flash, and 50 to 500 flashes for each record.

Nanosecond geminate reactions were followed using the same photolysis flash, arc, and cuvette holder. The arc was pulsed during observation by use of a four-element lumped

† T.Y. was supported by U.S. Public Health Service Grants HL 14508 and GM 48130. R.M.R. and Q.H.G. were supported by U.S. Public Health Service Grant GM 14276.

* To whom correspondence should be addressed.
‡ Jichi Medical School.
§ University of Pennsylvania.
|| Cornell University.

⊗ Abstract published in *Advance ACS Abstracts,* November 1, 1995.

0006-2960/95/0434-14658$09.00/0

parameter transmission line as described by Koechner (1988) and constructed in the laboratory, to give 200-fold brightening for about 50 μs. A fast photomultiplier (Hamamatsu R1219) was connected directly to a Tektronix 7104 oscilloscope with CCD camera.

Picosecond data were acquired by conventional pulse-probe technique using a delay line. The 7-ps, 30-mJ fundamental output of a YLF laser (Continuum, Santa Clara) was frequency doubled to 524 nm, and the beam was split to provide photolysis and observing pulses. The photolysis beam, 524 nm, whose path included the delay line, was reduced to 1 mm in diameter, and the fundamental removed with a filter. The maximum energy at the cell was approximately 2 mJ. A continuum was obtained by passing the pulse through a water cell. The beam was split, one half passing through the observation cell almost (<2°) colinearly with the photolysis beam. The reference beam was parallel and separated by 3 mm. Both beams were dispersed with a reflection grating (Jarrell Ash), and the spectra (half-bandwidth, 2 nm) focused on the active area of a CCD camera (Spectra Source Instruments). The sample was circulated through a 1-mm optical path cuvette attached to a 100-mL tonometer, to prevent cumulation of possible photolysis damage to the 1.2-mL sample. The effective rate of delivery of quanta, based on photolysis of COMb, was 2×10^{11} s^{-1}, a figure low enough to avoid serious damage effects. All picosecond data were acquired at room temperature.

Deconvolution of Picosecond Data. The raw spectra were converted to a series of difference spectra covering 30 nm in steps of 1 nm, and spaced at time intervals of 2 to 125 ps. To fit the data, concentrations of species were calculated with the assumption of a Gaussian flash, and that photodissociation is preceded by an ultra-rapid reversible step as described by Petrich et al. (1988). The photoproducts were assumed to return to the liganded state in two (or at most three) first-order processes. The spectra were taken one at a time, and the optimal weights to be applied to the calculated concentrations in order to reproduce the spectra were determined by least squares. The residuals for all 30 spectra were used to guide a conventional nonlinear program in optimizing the rate constants for the exponential decay of the photodissociated species, forming the normal equations in the usual way. Although the least squares step must find a local minimum in the response surface, a good representation of the data was usually achieved (as in Figure 10). The nickel reaction was represented separately as a single photochemical event followed by an exponential decay of the photoproduct.

In this way the parameters used to generate the calculated values of the concentrations were adjusted to minimize the differences between the calculated and observed spectra for all wavelengths and all time points. The main additional correction required is for group velocity dispersion in the continuum. The correction required, estimated to be 0.14 ps/nm, was approximated by following the development of bleaching in several blue dyes on a short time scale, assuming a single process. The procedure must be controlled by inspection of the output because there is no link between the chemistry and the rate constants, and because solutions may be found that are the difference between two similar large-amplitude spectra with opposite signs. In general, the number of parameters varied was limited to two or three, plus an alignment parameter relating the point of occurrence of the flash in the equations used to produce the calculated values to the real time of the flash.

Molecular Dynamics. The locally enhanced sampling protocol was used in the form implemented in the program MOIL (Elber et al., 1994). Ten ligand copies were used. The cutoff distance for the nonbonded interactions was 9 Å, and the 1−4 scaling factors for van der Waals and electrostatic interactions were 8 and 2, respectively. The time step was 2 fs, and all the bonds were "shaked" (Ryckaert et al., 1977). All crystallographic water molecules were included, modeled by TIP3P (Jorgensen et al., 1983). The equilibration period was 15 ps.

RESULTS

Kinetics of CO Binding to Ni−Fe Hybrids. The bimolecular reaction of the α-Fe hybrid is complex and is markedly dependent on the conditions of the experiment. The effect of pH is shown in Figure 1 (panels A and B). Data were collected by flash photolysis using a 9-ns flash, with two concentrations of CO and two levels of photolysis flash. Although not illustrated, some of the effects are due to the difference in composition of the buffer which was borate at pH 9.1 and 0.1M KP_i at pH 6.6. The time scales in Figure 1A (two concentrations of CO) were normalized by plotting the progress of the reaction against the integral of the concentration of free CO with respect to time. This is necessary because a given level of photolysis transfers the same amount of CO from the protein to solution, producing a larger fractional increase in free CO when the concentration before photolysis is lower. The effect of the transformation is to convert a time course arising from a second-order reaction (or from consecutive or parallel second-order reactions) to the form it would have had if the reaction(s) were first-order. The value of the ordinate is unaltered: the abscissa has the dimension of time × concentration, and, for the comparisons of Figure 1, was scaled by dividing the area under the curves by the (known) relative initial concentrations of CO. This permitted a fair comparison between the rate and form of the recombination time courses.

At pH 6.6, in Figure 1A, the second-order rates and time courses are very similar at the two concentrations of CO. The main component (0.95 of total absorbance change) has a rate of 0.15×10^6 M^{-1} s^{-1}.

The second-order rate is independent of fractional photolysis (Figure 1B). With the photolysis light reduced by a factor of 256, 11.6% of the bound CO was removed. The main second-order rate was 0.152×10^6 M^{-1} s^{-1} but the proportion of the faster component increased from 0.053 to 0.103. The fit remained excellent with a residual of 0.0004 in absorbance (0.39%).

The results for pH 9.1 are more complex. As shown in Figure 1A, in contrast to results at pH 6.6, the major component is fast, rather than slow. The scaling used shows the effect of CO concentration more clearly by eliminating the effect of the absolute rates. It is evident that the proportion of the rapid component is greater with high free CO during the reaction. Figure 1B shows that its proportion also depends on fractional photolysis, with the proportion of the faster component rising at low fractional photolysis. The results cannot, therefore, be described appropriately as a sum of independent second-order reactions. Experiments

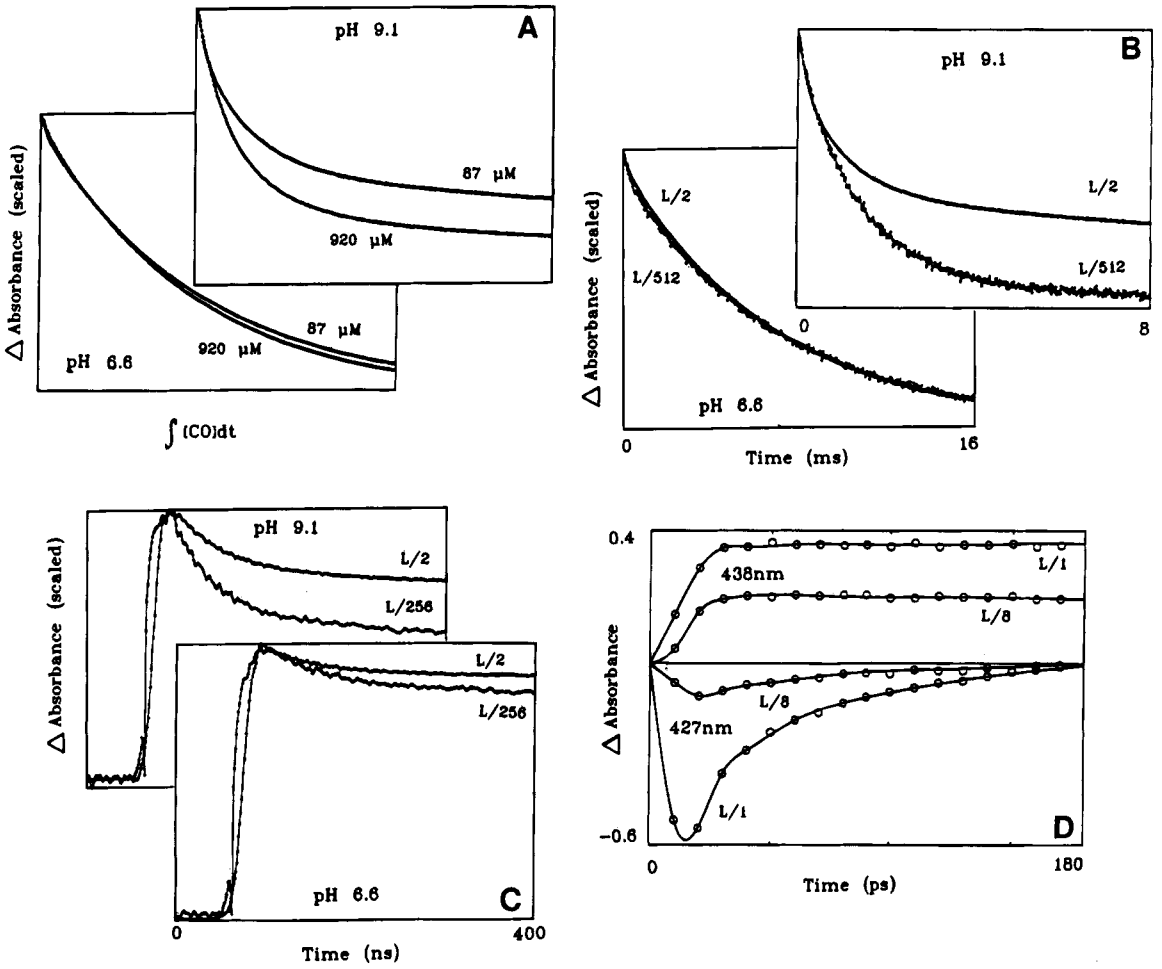

FIGURE 1: All data are for the α-Fe hybrid. (A) The effect of CO concentration on the rate and form of the time course of rebinding of ligand after photolysis with a 9-ns flash at 532 nm 30 times more intense than required to remove 50% of the ligand. The data were collected on time scales differing 10-fold, and have been adjusted to reflect the free CO after photolysis (details in text). The measuring wavelength was 436 nm, 20°, 0.1 M KP_i at pH 6.6, 0.1 M borate at pH 9.1. Heme at 56 μM, 1 mm path length. (B) The same solution; 920 μM CO, light levels as shown. (C) Geminate rebinding of CO, effect of pH and flash intensity. (D) Time course of absorbance change following photolysis with a 7-ps flash at 524 nm. Conditions: 0.1 M KP_i at pH 7.0, circulating cell, 1 mm path, light levels and wavelengths as shown; Fe followed at 438 nm, Ni at 427 nm.

at pH 7.3 using Tris−HCl + KCl buffer gave results similar to those at pH 9.

The nanosecond geminate reactions shown in Figure 1C show significant effects of the experimental conditions, with a doubling of the geminate amplitude for the α-hybrid at pH 9 as compared with pH 6.6. While the reduced amplitude of the geminate reaction at the large fractional photolysis shown in the figure may be explained in several ways, it must be due, in part, to the early completion of photolysis at high light intensity allowing rephotolysis of ligand molecules recombining during the lifetime of the flash.

Absorbance changes on a picosecond scale show two spectrophotometrically distinct kinetic components. One may reasonably be assigned to the appearance of unliganded heme, on the basis of its spectrum, and its persistence without change on this time scale (Figure 1D, upper part). The other component is presumably related to transient changes in the nickel porphyrin. The two spectra are readily separated, and the difference in the time course is obvious (Figure 1D, lower part). The apparent quantum yield of the two components is also different: Reduction of the intensity of the photolysis flash decreases the amplitude of the transient spectral change more than that of the persistent one (see center pair of records, panel D). The transient changes associated with nickel porphyrin do not show up in experiments in the nanosecond and microsecond ranges because the nanosecond photolysis flashes are not bright enough to generate a significant population of these species, given their low apparent quantum yield and short lifetime.

The results for CO binding to the β-Fe hybrid are quite similar to those for the α-Fe hybrid at the pH extremes of 6.6 and 9.1, but differ markedly at intermediate pH values. A number of experiments may be summarized by saying that at any pH value, the behavior of the β-Fe hybrid resembles that of the α-Fe hybrid at a significantly lower pH. The pH difference required is difficult to quantify, but it is at least 1 unit. The difference depends not only on pH but also on the composition of the buffer used: Data similar to those of Figure 2 can be obtained with the α-Fe hybrid only by combining the low pH of 6.6 with the use of phosphate buffers. The time course of bimolecular rebinding to the β-Fe hybrid is independent of fractional photolysis (Figure 2A). The form of the time course is independent of CO concentration, but the rate is proportional to it. The corresponding panels (Figure 1B, lower, and Figure 2A) are superimposable; thus both hybrids have the same the second-order rate constant (0.15×10^6 M^{-1} s^{-1}) at low pH. This simple behavior of the β-Fe hybrid is maintained up to pH

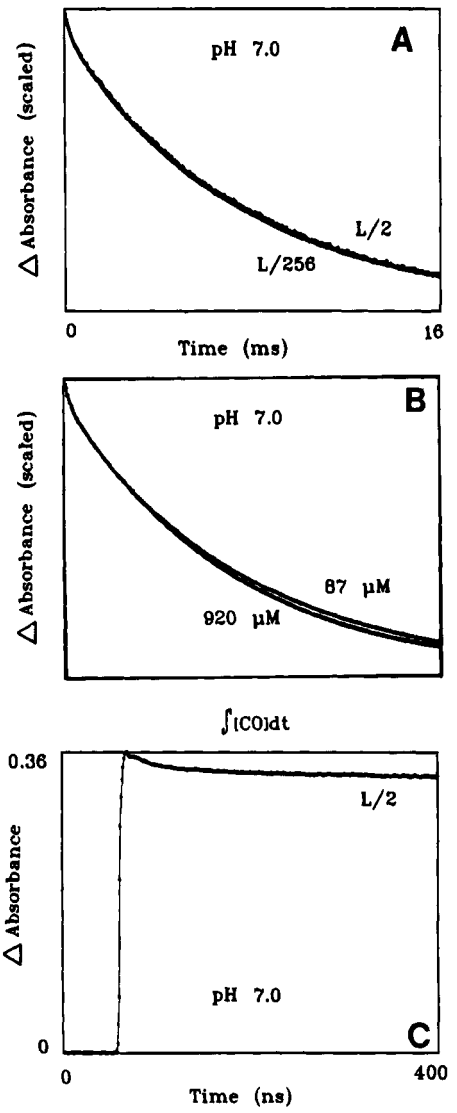

FIGURE 2: CO rebinding to the β-Fe hybrid. Conditions as for Figure 1 except that 0.1 M KP_i is at pH 7.0. (A) Effect of varying light intensity. (B) Effect of CO concentration. (C) Geminate recombination in the nanosecond range.

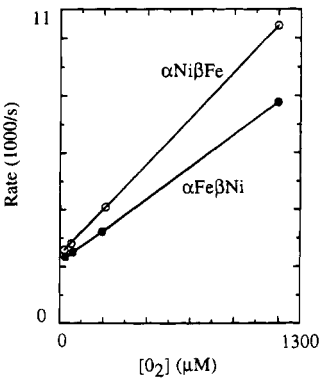

FIGURE 3: Observed first-order rates of absorbance change after flash photolysis of oxy-hybrids. Conditions: 0.1 M KP_i, 20°, heme 50 μM. Observation at 436 nm, 1 mm path, 9 ns flash. The ordinate gives the apparent rate in thousands per second, the abscissa initial oxygen concentration in μM.

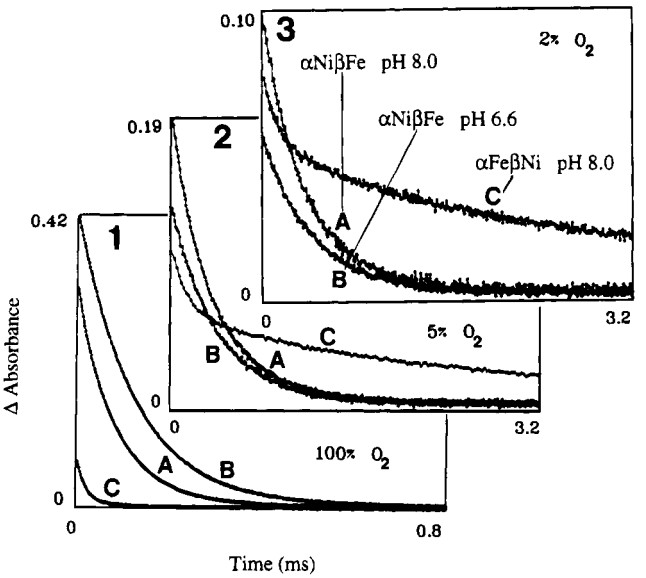

FIGURE 4: Combination of oxygen with α-Fe and β-Fe hybrids. Data are shown for 0.1 M KP_i at pH 6.6 and Tris-HCl + 0.1 M KCl at pH 8.0 for the β-Fe hybrid, and for Tris-HCl−KCl at pH 8.0 for the α-Fe hybrid. Three oxygen concentrations were used: Panel 1: 100% O_2; (A) β-Fe, pH 8.0; (B) β-Fe, pH 6.6; (C) α-Fe pH 8.0. Panel 2: 5.1% O_2; A, B, and C as for panel 1. Panel 3: 2.0% O_2; A, B, and C as for panel 1.

8, but in borate buffer at pH 9 its behavior changes and closely resembles that of the α-Fe hybrid at intermediate pH values. Insofar as comparisons can be made, bimolecular CO binding to the nickel hybrids is very similar to binding to Mn−Fe hybrids as reported by Blough et al. (1984).

Nanosecond geminate rebinding is similar to that of the α-Fe hybrid at low pH (Figure 2C), and picosecond experiments also give similar results, which differ somewhat in the nickel contribution.

Reactions of Hybrids with Oxygen. There is a clear analogy with carbon monoxide in the reactions of the two hybrids with oxygen. The simplest case is illustrated in Figure 3, which shows the rate of reequilibration after photolysis as a function of oxygen concentration for both hybrids in 0.1 M KP_i at pH 6.6. The results are not identical, but the differences are not large. Extrapolation to zero oxygen concentration suggests a rapid rate of dissociation of oxygen of the order of 2000 s^{-1} in both cases. The slopes of the lines lead to second-order rates of 4.8 and 7.5 × 10^6 M^{-1} s^{-1} for α- and β-Fe hybrids, respectively.

Large differences between the hybrids appear at higher pH values; the panels of Figure 4 show data at three oxygen concentrations for the α-Fe hybrid at pH 8 and for the β-Fe hybrid at pH 6.6 and 8. At 1 atm O_2, the excursion observed for the β-Fe hybrids is some 4 times greater than that for the α-Fe hybrids (Figure 4, panel 1, B: β-Fe; C: α-Fe hybrid). The effect of pH on the amplitude for the β-Fe hybrid (panel 1, A and B) is consistent with the oxygen equilibrium data of Shibayama et al. (1986), which suggest a saturation of about 80% with 1 atm O_2 at pH 6.6.

With 0.05 atm oxygen, the absorbance excursion associated with the α-Fe hybrid (Figure 4, panel 2, C) has increased relative to that of the β-Fe hybrid (panel 2, A and B), and has become markedly biphasic. The trend continues at the lowest oxygen partial pressure used (0.02 atm), where the very slow reaction of the α-Fe hybrid now dominates its relaxation (panel 3, C).

These findings may be described qualitatively in terms of a two-state model by assuming that the β-Fe hybrid is almost wholly in a low-affinity state, with or without ligand, in the experiments at pH 6.6, and is largely in the same state even

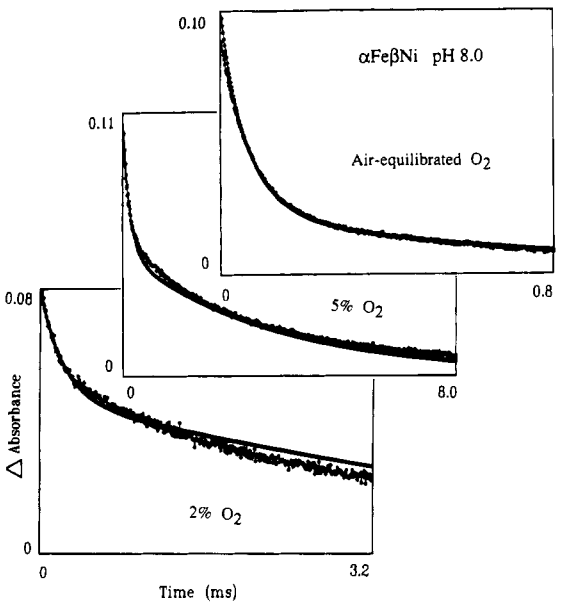

FIGURE 5: Comparison of observed and computed results for the reaction of O_2 with α-Fe hybrid. The data are taken from Figure 4. The continuous lines were computed with the same parameter values for the three oxygen concentrations. The two-state model of Monod et al. (1965) was used with explicit rates of interconversion between R and T states. The allosteric L = 1.7×10^3, *c* (calculated from rate parameters) = 607 (final values), rate $R_o \rightarrow T_o = 2.4 \times 10^4\ s^{-1}$, $T_o \rightarrow R_o = 14\ s^{-1}$, $R_1 \rightarrow T_1 = 1000$, $T^1 \rightarrow R^1 = 350$, $R_2 \rightarrow T_2 = 40\ s^{-1}$, $T_2 \rightarrow R_2 = 8600\ s^{-1}$, $T_{on} = 8.7\ \mu M^{-1}\ s^{-1}$, $R_{on} = 48.5\ \mu M^{-1}\ s^{-1}$, $T_{off} = 2200\ s^{-1}$, $R_{off} = 20.6\ s^{-1}$. Quantum yield for T = 0.99, quantum yield for R = 0.38. Root mean square residual = 0.0027 in absorbance.

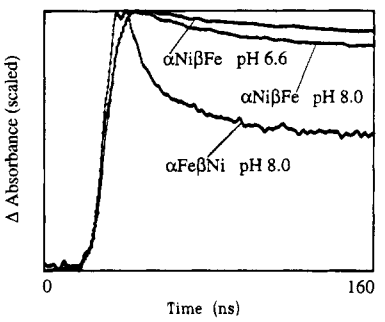

FIGURE 6: Nanosecond geminate reactions. Conditions as for Figure 4 but with 100% O_2. Hybrids and conditions as shown.

at pH 8. The α-Fe hybrid is in a high-affinity state at pH 8 when liganded, but when unliganded, converts to a low-affinity state. With the highest oxygen (panel 1, C), the α-Fe hybrid remains in the high-affinity state throughout the photolysis and recombination cycle, as there is not enough time to allow change of state before ligand rebinding.

The low apparent quantum yield (small absorbance excursion on photolysis) with 1 atm O_2 is due, in part, to nanosecond recombination (Figure 6), and also to a much faster reaction competing with the photolysis flash, leading to a nanosecond amplitude about 40% of that for the β-Fe hybrid. (The data in Figure 6 have been scaled to show the form of the relaxation. The difference in the time course of ligand removal as monitored at 436 nm also reflects this rapid reaction, and is not artifactual.)

The two-state model has been applied quantitatively, fitting the time course at the three lowest oxygen concentrations with the results shown in Figure 5. To begin with, the concentrations of intermediates before photolysis were computed from the rate and allosteric parameters. In photolysis, the amplitude of geminate recombination of the two forms was modeled by using different quantum yields for the high- and low-affinity forms, and the concentrations of intermediates were given by a binomial distribution. The rates of allosteric interconversion were explicit. The data could be represented quite reasonably in this way in terms of rate and amplitude, implying that the oxygen equilibrium curve is fitted as well as the kinetic data. The allosteric parameters are not fully defined, however, as a two-state model requires three parameters to fit an equilibrium curve, while an equation equivalent to the Adair equation requires only two. The asymptotes of an equilibrium curve do not represent the behavior of pure allosteric states, and an indefinite number of pairs of L and c values is possible. The values used are listed in the legend to Figure 5. It may be noted that both on and off rates for the high-affinity form are reasonably close to those for human hemoglobin A; the preferred value of the allosteric parameter L, 1.7×10^3, is small as expected for a phosphate-free buffer (Eaton et al., 1991), while c is large. The values for T-state on and off have large errors; the data can also be represented, supplying the values from Figure 3, as fixed input without changing the allosteric parameters, though the fit is not quite as good as is shown in Figure 5 (root mean square residual about 10% greater).

Nanosecond Oxygen Reaction. The data presented in Figure 6 are consistent with the results of the other experiments with oxygen. It is particularly noteworthy that the β-Fe hybrid shows scarcely any geminate rebinding at pH 6.6, and only slight rebinding at pH 8.0. The smooth ending of photochemical removal of oxygen shows that there is no rapid reaction competing with the photoflash. In contrast, the α-Fe hybrid shows an earlier and sharper ending, suggestive of a rapid reaction, and the amplitude (Figure 6 is scaled) is only about half as great as for the other hybrid under similar conditions.

Picosecond experiments with O_2 are more difficult to deal with than those with CO both because it cannot be assumed that there is no picosecond geminate reaction, and because the effective quantum yield for oxygen dissociation is lower than that for CO, leading to greater interference from nickel. In addition, there is a large transient difference spectrum (Greene et al., 1978) which follows photodissociation of oxygen from hemoglobin. These components could not be extracted reliably from the time-resolved spectra for the oxygenated hybrids alone.

In an attempt to introduce some chemical information to the deconvolution process, photochemical difference spectra were first measured for deoxy α-Fe•β-Ni hybrid. This gives a large excursion broadly similar to the spectra shown in Figure 9 for the NO hybrid, with bleaching at the Ni maximum of 420 nm. It disappears over the next nanosecond and may be due to breaking the Ni-proximal histidine bond. Data were collected for ordinary oxyhemoglobin A over the same range of time and wavelength. The spectra for hemoglobin A were decomposed into two components, one representing ligand binding, the other the transient spectrum of Greene et al. (1978). Finally, the experiment was repeated with the oxygenated α-hybrid. The difference spectra for the deoxy α-Fe hybrid, and the difference spectra for HbA were used to represent the time-resolved difference spectra for the oxygenated α-Fe hybrid. The weight given to each

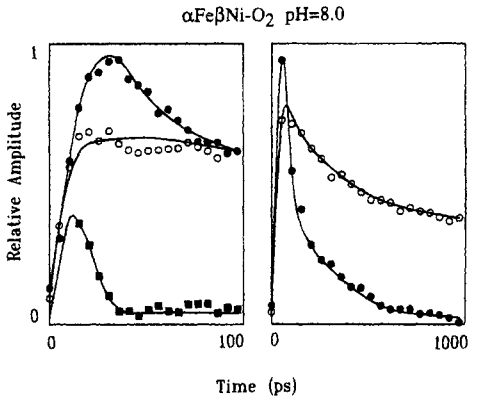

FIGURE 7: Time courses for Ni relaxation (filled circles), and deoxy-Fe (open circles) following flash photolysis of the α-Fe hybrid. The scale of the traces is arbitrary (see text). Data for two time scales are shown. The filled squares give the time course for the intermediate of Greene et al. (1978).

of the components as a function of time was taken to be proportional to its concentration, with the results shown in Figure 7. The figure shows the progress curve for the concentration of deoxyhybrid (open circles), and nickel transient (filled circles). The Greene et al. (1978) species is shown for the shorter time figure as filled squares. The procedure does not give any indication of the absolute concentration of any of the components; only the changes are meaningful. The results are consistent with a picosecond oxygen rebinding reaction. The assumptions involved are quite serious, however, especially as the fraction of the total absorbance change attributable to the oxygen reaction is outweighed by the transient changes in the nickel spectrum.

The β-Fe hybrid did not show picosecond rebinding of oxygen either at pH 6.6 or at pH 9. After the first tens of picoseconds, the only absorbance changes were those of the nickel porphyrin.

Reaction of Hybrids with Nitric Oxide. The second-order reaction measured by flash photolysis gave a rate of 8×10^6 M^{-1} s^{-1} for the α-Fe hybrid at pH 6.6 and 18×10^6 M^{-1} s^{-1} at pH 9. The rate measured at pH 6.6 was not affected by the addition of 5 mM inositol hexaphosphate. The rate for the β-Fe hybrid was 3.3×10^7 M^{-1} s^{-1} both at pH 7.0 and at pH 6.6. The rates for the β-hybrid are of the same order as that for hemoglobin A (Cassoly & Gibson, 1975). The main problem in performing the experiment is the low apparent quantum yield of the proteins. This applies particularly to the α-Fe hybrid, where the absorbance change available for measurement is very small. The apparent quantum yield for the β-hybrid, though still much lower than that for oxygen, is 10 times greater than for the α-hybrid in experiments at pH 6.6 with phosphate buffer. Numerical values are on the order of 0.001 and 0.01 for α- and β-hybrids, respectively.

Experiments in the nanosecond range could be performed satisfactorily with the β-hybrid only at pH 6.6. At pH 9, although there is a small relaxation closely following the flash profile, a check of its spectrum showed that it is substantially attributable to nickel. Data for the β-Fe hybrid are shown in Figure 8. They are well represented by a rate of 4.8×10^7 s^{-1}, 85% of amplitude, and a rate of 1.5×10^6 s^{-1} accounting for 15%. The second rate is an underestimate since its associated amplitude includes second-order binding which is much slower still in the conditions of the experiment.

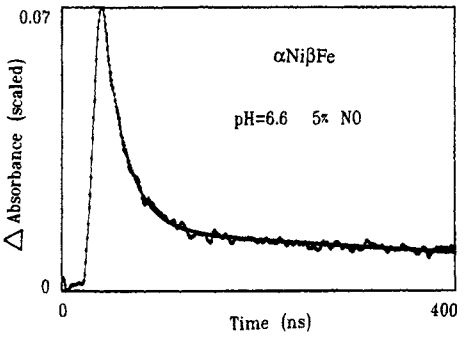

FIGURE 8: Nanosecond geminate reaction of β-Fe hybrid. The flash starts near the left edge of the figure; removal as well as rebinding of the ligand is shown. The continuous line is a fit to a sum of exponentials. Observation at 436 nm, 1 mm, 50 μM heme, 9 ns flash. The maximum excursion corresponds to 15% of the total bound NO.

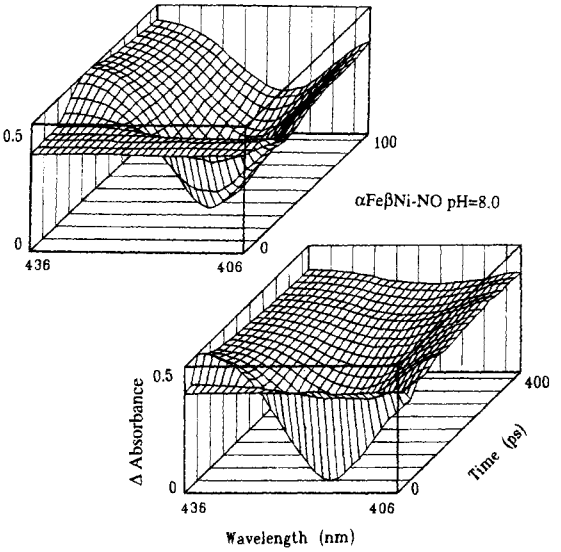

FIGURE 9: Time-resolved difference spectra for the α-Fe hybrid NO. For the upper box, the separation between spectra is 5 ps, and for the lower box it is 20 ps. The 7 ps flash begins at 10 ps.

Picosecond rebinding of NO, though difficult to follow, is important for defining the controlling factors in the reaction of the hybrids with ligands. The problems are illustrated in Figures 9 and 10 which show the evolution of the spectra for the α-Fe hybrid on two time scales following photolysis, and their decomposition into kinetic components. When the spectra are separated by 5 ps (upper left in Figure 9) the initial baseline before the flash is succeeded by both positive and negative excursions. The negative excursion is 4 to 5 times larger than the positive one, and has its greatest value around 420 nm. The positive one is maximal at the longer wavelength limit of the figure at 436 nm, where a relaxation is readily seen from 50 to 100 ps. This does not account for much of the total change, as at 100 ps the difference spectrum is still far from the baseline. The lower right panel shows that return to the initial state has been largely completed by 400 ns.

The data were then analyzed to separate the kinetic components and their spectra. A part of the result is shown in Figure 10. The left-hand block of tiles shows the observed time course of the absorbance change at each of 20 wavelengths, nanometer by nanometer. The scale of the ordinate is the same in all of them: The first tile represents the longest-wavelength element in Figure 9. The points are

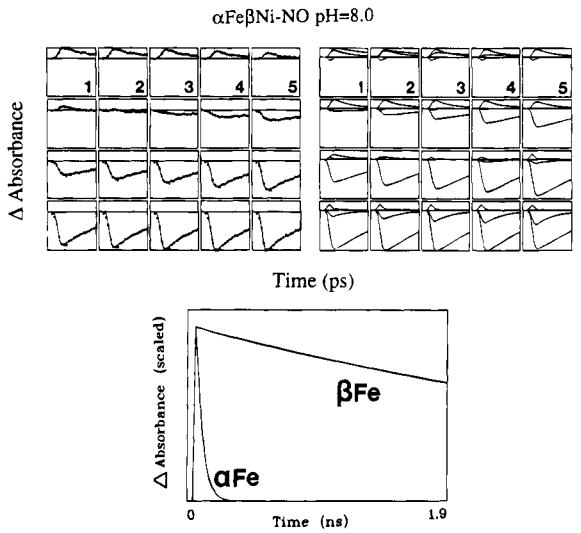

FIGURE 10: The left-hand block of 20 titles shows the progress curves for wavelengths from 436 nm (1) to 417 nm following photolysis of α-Fe•NO. The points are separated by 5 ps. The scale is the same for all tiles. The lines do not connect the points but were calculated as described in the text. The right-hand block shows the weight given at each wavelength to each of three time courses. The faster component represents NO rebinding, the larger slower component is Ni relaxation. The lower panel compares the computed time courses of NO picosecond rebinding to α- and β-hybrids at pH 6.6.

experimental, the lines computed. The right-hand block of tiles shows the relative weights given to the kinetic components in the analysis. Inspection shows two major components with different rates of disappearance and different isosbestic points.

An analogous experiment performed using the deoxy α-Fe hybrid showed only one difference spectrum with a rate similar to that of the larger component in Figure 9. This component is attributed to the Ni-porphyrin. The isosbestic point for the smaller component (in the third element of column 3, Figure 10) is consistent with its identification with NO rebinding. The rate at pH 6.6 is 18 ns^{-1}; and at pH 8, 25 ns^{-1}.

Similar considerations apply to determinations with the β-Fe hybrid. Both the rate of the Ni relaxation and its wavelength are somewhat different from those of the α-Fe hybrid. The course of NO rebinding at pH 6.6 includes a component with the unusually low rate of 0.5 ns^{-1}. The rate at pH 9 was 10 ns^{-1}. It is difficult to give estimates of the probable errors, which are not normally distributed because of the existence of multiple minima in the nonlinear least squares estimation. The standard error for the NO rate related to a single minimum appears to be quite small, and may not be more than 10%. In this procedure, it is essential to look carefully at the spectra and tiles of the form shown in Figure 10, together with the matrix of correlations between the parameters being varied.

Molecular Dynamics. Simulations, using the program MOIL (Elber et al., 1994), usually for 50 ps of computed time, were carried out for the α-Ni•β-Fe hybrid from the coordinates of Luisi et al. (1990), including all crystallographic water molecules, as a starting point. The results were unusual in that, using the locally enhanced sampling algorithm, the group of ligands moved quickly away from the iron atom in each of 8 runs started with a different initial distribution of velocities. Their motion was toward Ile-106 and Leu-28, and away from His-63 and Val-67 in each case. This unusual behavior may be correlated with the crystallographic finding of close contacts between the ligand and His-64 Nε, and between the ligand and Val-67 Cγ. In all but one run, the ligands remained in this new position without returning to the iron atom. This behavior is summarized in Figure 11, which shows the ligands and spaces around the iron at 1 and 4 ps after starting dynamics. Although the total accessible volume is relatively large, it is remote from the iron, and is consistent with the low rate (0.3 ns^{-1}) of NO rebinding measured for this hybrid at low pH.

Simulations of the α-Fe hybrid cannot be started from the crystal structure, which is not available. Attempts to use the deoxy structure of hemoglobin A (Fermi et al., 1984) did not lead to satisfactory results, with ligands escaping freely from the anhydrous molecule. As an approximation, the structure of Luisi and Shibayama (1989) for the α-Fe•β-Co hybrid was taken as a starting point. An example of the results is included in Figure 11 (panel A). The ligands are more tightly held than in the α-Ni hybrid, and are closer to the iron, so the expected rate of recombination of NO would be higher than for the α-Ni•β-Fe hybrid, as was observed experimentally at both pH 6.6 and pH 9.

As a control, simulations were run for native liganded (R-state) hemoglobin using the coordinates kindly made available by Dr. Paul Emsley (Derewenda et al., 1990). The results showed little difference between the subunits, and generally resemble the behavior of the α-Fe hybrid more closely than that of the β-Fe one. These results are shown graphically in Figure 12 which compares the numbers of close approaches to the iron during the 50-ps simulation. It is obvious that the β-Fe hybrid is markedly different from the others.

DISCUSSION

In describing the results, we have used the two-state model of Monod et al. (1965) qualitatively, and to some extent, quantitatively. In the model, the T and R states are abstractions which, in studies with hemoglobin, are frequently equated with its deoxy and liganded forms as defined by X-ray crystallography. When one is considering the nickel−iron hybrids, this is appropriate for the T-state, as both deoxy hybrids are believed to be similar in structure to deoxy HbA (Luisi & Shibayama, 1989; Luisi et al., 1990). When it is necessary to postulate high-affinity forms of the hybrids, although these are called R-forms, this does not imply that their structures are similar to those of the R-form of HbA.

The two-state model postulates an equilibrium between T and R states where $T_n = L \cdot c^{-n} \cdot R_n$; n is the number of ligand molecules bound, and c is the ratio of the affinities of the R and T states expressed as association constants. As c is often on the order of 500, the equilibrium shifts correspondingly towards the R-state as ligand binding proceeds. Within each state ligand binding is fully described by a single binding constant.

As noted in the introduction, binding of CO to the nickel hybrids has been reported by Murray et al. (1988, 1989), with results interpreted qualitatively in terms of the two-state model. In addition, Blough et al. (1984) have reported detailed studies of CO rebinding to Mn−Fe hybrids, treating their results quantitatively in terms of a two-state model. The

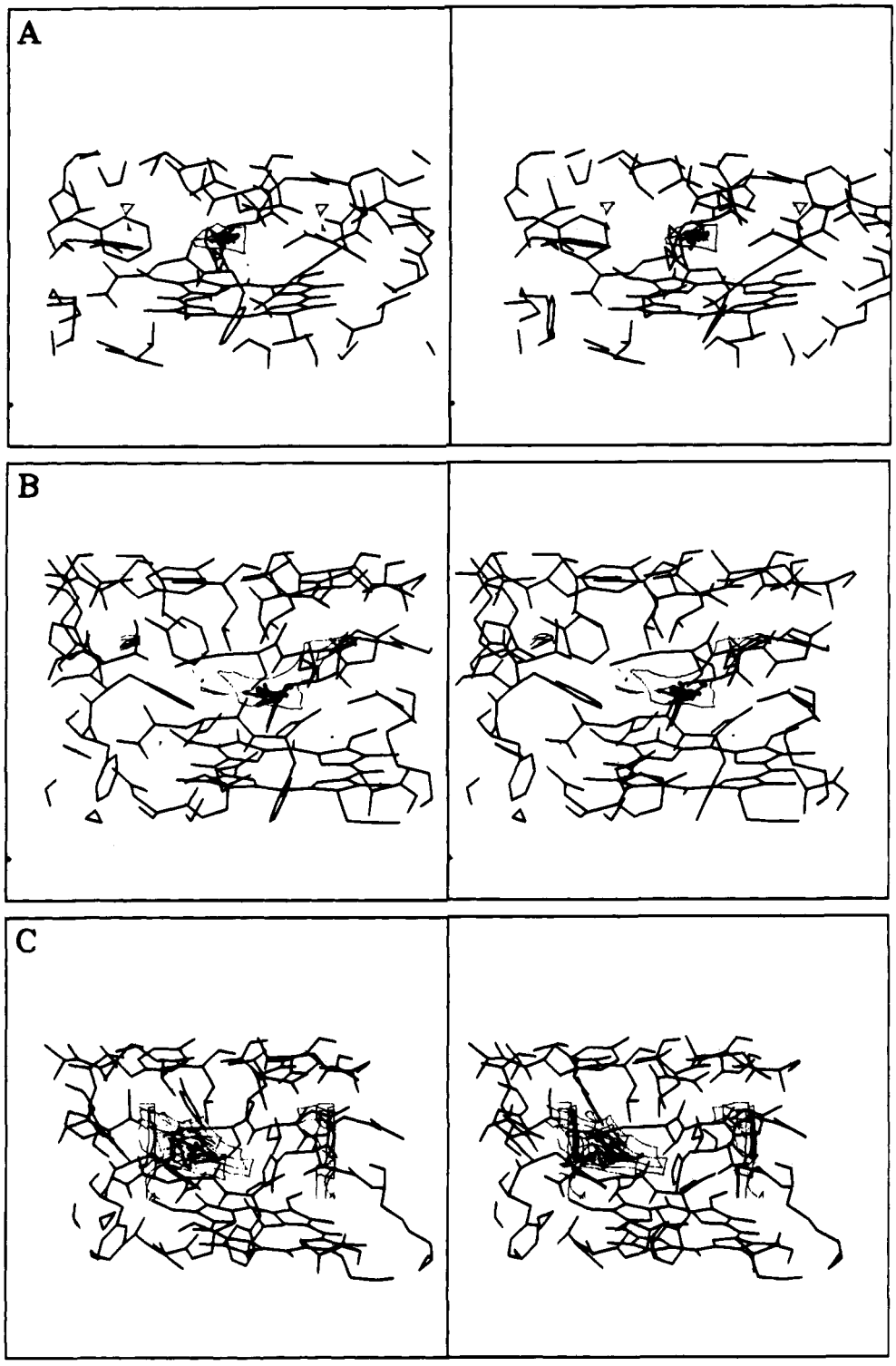

FIGURE 11: Stereo diagrams of atomic positions and spaces near the heme pocket during molecular dynamics simulations. The direction of view is between the heme propionates with the distal histidine toward the observer, Phe CD1 to the left, and Val E11 to the right. The ligands are shown as bars with dots at the end. Spaces able to accommodate a ligand molecule are indicated by light lines. These contours are drawn at intervals of 1 Å along the z-axis. The chosen volume was populated by atom, not by residue. (A) α-Fe hybrid 15 ps into simulation; (B) β-Fe hybrid, 1 ps; (C) β-Fe hybrid, 4 ps.

results for CO reported here confirm the earlier data, and add other evidence of cooperativity in both α- and β-Fe hybrids.

Specific results with CO and O_2 are discussed next in relation to relevant kinetic observations with HbA. The question of functional differences between the α- and β-subunits has a long history, reviewed in detail by Ho (1992). Carbon monoxide binding was studied by Parkhurst et al. (1970), who labeled the subunits of HbA by replacing α- or β-protohemes with meso and deutero hemes, whose spectra are significantly different. The course of CO binding to each type of subunit could be followed independently. The results suggested equivalence of the subunits in T-state binding. There was no sign of a compulsory order of binding, and especially with mesoheme, little overall effect of the substitution. The data presented here for the hybrids

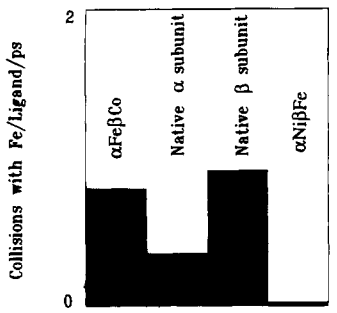

FIGURE 12: Count of close approaches of ligand atoms to heme iron. The total numbers of approaches to less than 4 Å were counted for 8 runs of 50 ps each for the hybrids and for R-state HbA. The average is plotted. The maximum possible would be 2 if all ligands remained within 4 Å of the iron throughout the simulation.

confirm this result. This does not agree with the much quoted speculation (Perutz, 1970) that ligands should not bind to β-subunits in the T-state. The β-subunits certainly bind CO, O_2, and NO, and are equally certainly in the T-state structure in the crystal (Luisi & Shibayama, 1989).

Experiments performed with oxygen at pH 6.6 show a difference between the hybrids which is outside experimental error, but it is not large. With oxygen, the overall rate of dissociation is an important factor in determining the behavior of the T-state hybrids, and this rapid rate, too, is similar for both. The difference between the two hybrids, as has already been said, lies in their response to a pH change, the β-hybrid requiring a much higher pH to display cooperativity.

The most immediately relevant experiments with hemoglobin A and oxygen are those of Sawicki and Gibson (1977), who reported several relaxations in experiments in 0.1 M KP_i at pH 7.0, interpreted by use of an extended Monod et al. (1965) model including α-β differences and dimers. The low stability of their Zr arc light source limited the observations to short time periods. They assigned their fastest relaxation to the β-subunits, with on and off rates of 12×10^6 M^{-1} s^{-1} and 2500 s^{-1}, respectively. The α-subunits were thought to have smaller rates in both directions of 3×10^6 and 200 s^{-1}. Later work (C. A. Sawicki & Q. H. Gibson, unpublished) with an improved apparatus confirmed the earlier observations, but showed that rather than two major relaxations, there were actually three, the slowest at 20 to 30 s^{-1}. This low rate could not be modeled in computations using the two-state model. It was also found that adding inositolhexaphosphate simplified the results, with the largest part of the reaction now being accounted for by the fastest relaxation.

Although data for the oxygen reactions of the hybrids have not been obtained under precisely the conditions used by Sawicki and Gibson (1977), the sum of expected behaviors of the α- and β-hybrids at low oxygen tensions are qualitatively similar to the data for hemoglobin A, suggesting that their deoxy forms may be a good model for T-state deoxy hemoglobin A. It has been shown that the data for the α-Fe hybrid may be represented by a two-heme two-state model (Figure 5). The value of L, the ratio between the concentrations of the T-deoxy and R-deoxy forms, in the example shown, was 24 000 for the α-hybrid, and, as the value of c is 607, a change to the R state would be expected for the doubly liganded form. The rates for the β-Fe hybrid at the limiting pH values of 6.6 and 9.1 are similar to those for the α-Fe hybrid, so c must also be similar. Under the conditions of Figure 5, however, the kinetics show that the doubly liganded β-Fe hybrid must be largely in the T-state, calling for $L > c^2$, that is substantially more than 360 000. While L may indeed be larger for the β-Fe hybrid, in hemoglobin A, the two-state model allows only a single value for L, requiring that the behavior of the two subunits be alike.

An obvious extension is to replace it with a three-state scheme, as has been proposed from time to time. Such a change would be consistent with the work of Marden et al. (1986), who combined absorption measurements of saturation and fluorescence measurements on an effector during CO rebinding after photolysis. The standard two-state model predicts that a fluorescent effector will bind more strongly to the T-state and will be released to the solution on ligand binding. By definition, however, this release can happen only at the rate of CO binding to the T-state; that is, it will be slow. Experimentally, however, especially at low pH, there is substantial release of effector at the R-state rate, implying an intermediate with T-state effector binding, but with an R-state CO binding rate. Analysis showed that the second molecule of ligand was involved. This result would be explained if there is a third state where the α-subunits interact, changing the rate of ligand binding, but the main T to R conformation change releasing an effector has not taken place.

A pH-sensitive third state can accommodate another kinetic anomaly of long standing. In the first reasonably precise measurements of the time course of CO binding to sheep hemoglobin, Gibson and Roughton (1957) found that when binding was represented by four consecutive reactions, at pH 9 the second rate constant had to be made larger than the first, whereas at pH 7 the first two rates were the same, and the third was larger (the fourth was set to the R-state value). This apparently implausible result follows directly from the results for the two hybrids, with the α-subunit providing faster binding at pH 9 before the occurrence of the general R to T transition. It may be added that the normal two-state model, which naturally leads to monotonically increasing rate constants, is inconsistent with the kinetic experiments at pH 9.

The explanation of Sawicki and Gibson's anomaly is slightly more complex. The expected sequence of kinetic events is that, depending on pH, oxygen will be distributed randomly among the subunits of deoxyhemoglobin. Doubly liganded α-subunits are favored by cooperativity between the α-subunits (giving the third allosteric state); the rate of ligand redistribution, however, will be low. It will be limited by the multiple steps in which ligand dissociates from an α- or a β-subunit, and binds to a singly liganded α-subunit as the second ligand molecule, held after the appropriate conformation change with R-state affinity.

Data for the Reactions of the α-Hybrid with NO. The second-order and nanosecond reactions are difficult to measure because so little ligand escapes from the heme, and in the nanosecond range Ni adds a rapid component. The picosecond geminate reactions range beween 10 and 35 ps^{-1}. The bimolecular reaction (5×10^6 M^{-1} s^{-1}) is unusually slow.

The β-Fe hybrid has a second-order rate (33×10^6 M^{-1} s^{-1}), somewhat below the O_2 R-state rate of 50 M^{-1} s^{-1} for

HbA (Gibson & Edelstein, 1987), and the nanosecond geminate rate of 5×10^7 s^{-1} is also low. The most striking result, however, is that the picosecond rate is too low to measure conveniently with a pulse-probe apparatus, but is on the order of 0.5×10^9 s^{-1} (Figure 10, lower panel).

These results indicate that ligands can diffuse into the interior of the β-hybrid faster than into the α-hybrid, but that, once in the protein, reaction is more likely to follow in the case of the α-hybrid than in the β-hybrid.

Finally, the molecular dynamics results permit proposals for the kinetic origins of the change in affinity associated with the R−T transition. The β-Fe hybrid is unusual in that the ligand molecule moves rapidly away from the iron, leaving no open return pathway behind it. Panels B and C of Figure 11 show the outlines of spaces within the protein large enough to accommodate a ligand molecule. At 1 ps, the ligand cloud is already moving away from the iron, and at 4ps (panel C) has moved into a large space which has opened up some 8 Å from the heme iron. This is consistent with the very low rate of NO geminate recombination observed experimentally. The rate of CO binding should be lowered to about the same extent, without requiring a change in the reactivity of the heme iron. At least a part of the characteristically high overall rate of oxygen dissociation may be related to the same molecular dynamics observation. The difficulty in returning to the iron causes a higher proportion of thermal dissociation events to be effective in bringing about escape from the protein molecule. In other words, geminate recombination at all time ranges should be less in the T-state, as is, indeed, observed. The suggestion is that at least some of the R−T differences are to be accounted for by the details of the structure on the distal side of the heme. The simulations also suggest that, besides the effect of the short contacts with His-63 and Val-67, the movements of residues needed to open up the spaces seen in Figure 11C, to the left of and above the heme determine the paths of the ligands in the β-Fe hybrid.

Although the rate of picosecond geminate NO recombination to the β-hybrid is low by comparison with that of other hemoproteins, the absolute rate of 5×10^8 s^{-1} is still high enough to support a very high second-order rate for biomolecular NO binding. It is fast enough to let the bimolecular rate be taken as a measure of diffusion from the exterior of the protein to the heme pocket. This bimolecular rate is in the same range as that for the R-state native protein and for many myoglobins.

Comparison of the molecular dynamics results for the β-Fe hybrid with those found starting from the native R-state CO coordinates, and from the α-Fe•β-Co structure, shows that the ligands are held closer to the heme than in the β-Fe hybrid and have a smaller accessible volume (Figure 11A). As a result, the number of close approaches to the iron is larger, and, for the α-Fe•β-Co hybrid is in the same range as that for the R-state native structures. Unusually, the α-hybrid shows a picosecond geminate reaction with oxygen (Figure 7). The experimental results with both ligands are consistent with the simulation.

In conclusion, it seems reasonable to accept the Ni−Fe hybrids as a models for the T-state of hemoglobin A. While the β-subunits may remain in the T-state even when liganded, over most of the physiological pH range, the α-subunits develop intrapair cooperativity, consistent with an additional allosteric state other than the R and T states.

REFERENCES

Alston, K., Schecter, A. N., Arcoleo, J. P., Greer, J., Parr, G. R., & Friedman, F. K. (1984) *Hemoglobin 8* (1), 47−60.

Blough, N. V., Zemel, H., & Hoffman, B. M. (1984) *Biochemistry 23*, 2883−2891.

Cassoly, R., & Gibson, Q. H. (1975) *J. Mol. Biol. 91*, 301−313.

Derewenda, Z., Dodson, G., Emsley, P., Harris, D., Nagai, K., Perutz, M., & Reynaud, J.-P. (1990) *J. Mol. Biol. 211*, 515−519.

Eaton, W. A., Henry, E. R., & Hofrichter, J. (1991) *Proc. Natl. Acad. Sci. U.S.A. 88*, 4472−4475.

Elber, R., Roitberg, A., Simmerling, C., Goldstein, R. F., Verkhiver, G., Li, H., & Ulitsky, A. (1994) MOIL: A molecular dynamics program with emphasis on conformational searches and reaction path calculations, in *Statistical Mechanics, Protein Structure and Protein Substrate Interactions* (Doniach, S., Ed.) pp 165−191, Plenum Press, New York.

Fermi, G., Perutz, M. F., Shaanan, B., & Fourme, R. (1984) *J. Mol. Biol. 1F55*, 495−505.

Gibson, Q. H., & Roughton, F. J. W. (1957) *Proc. R. Soc. London, Ser. B 146*, 206−224.

Gibson, Q. H., & Edelstein, S. J. (1987) *J. Biol. Chem. 262*, 516−519.

Greene, B. I., Hochstrasser, R. M., Weisman, R. B., & Eaton, W. A. (1978) *Proc. Natl. Acad. Sci. U.S.A. 75*, 5255−5259.

Ho, C. (1992) *Adv. Protein Chem. 43*, 152−312.

Jorgensen, W. L., Chandrasekhar, L., & Madura, J. D. (1983) *J. Chem. Phys. 79*, 7270−7286.

Koechner, W. (1988) in *Solid State Laser Engineering*, p 301, Springer, Berlin.

Luisi, B., & Shibayama, N. (1989) *J. Mol. Biol. 206*, 723−736.

Luisi, B., Liddington, B., Fermi, G., & Shibayama, N. (1990) *J. Mol. Biol. 214*, 7−14.

Manoharan, P. T., Alston, K., & Rifkind, J. M. (1989) *Biochemistry 28*, 7148−7153.

Marden, M. C., Hazard, E. S., & Gibson, Q. (1986) *Biochemistry 25*, 7591−7596.

Monod, J., Wyman, J., & Changeux, J.-P. (1965) *J. Mol. Biol. 12*, 88−118.

Murray, L. P., Hofrichter, J., Henry, E. R., Ikeda-Saito, Kitagishi, K., Shibayama, N., Yonetani, T., & Eaton, W. A. (1988) *Biophys. J. 53*, 629a.

Murray, L. P., Henry, E. R., Hofrichter, J., Shibayama, N., Yonetani, T., & Eaton, W. A. (1989) *Biophys. J. 55*, 55a.

Parkhurst, L. J., Geraci, G., & Gibson, Q. H. (1970) *J. Biol. Chem. 245*, 4131−4135.

Perutz, M. F. (1970) *Nature 228*, 726−739.

Petrich, J. W., Poyart, C., & Martin, J. L. (1988) *Biochemistry 27*, 4049−4060.

Ryckaert, J. P., Ciccotti, G., & Berendsen, H. J. C. (1977) *J. Comput. Phys. 23*, 327−341.

Sawicki, C. A., & Gibson, Q. H. (1977) *J. Biol. Chem. 252*, 7538−7547.

Shelnutt, J. A., Alston, K., Ho, J.-Y., Yu, N.-T., Yamamoto, T., & Rifkind, J. M. (1986) *Biochemistry 25*, 620−627.

Shibayama, N., Morimoto, H., & Miyazaki, G. (1986) *J. Mol. Biol. 192*, 323−329.

BI951308J